Application of scaled boundary finite element method for vibration-based structural health monitoring of breathing cracks

Naserodin Sepehry[1], Mohammad Ehsani[2,3], Weidong Zhu[4] and Firooz Bakhtiari-Nejad[3,4]

Abstract

The dynamic response of the host structure to a high-frequency actuation is usually used for the detection of tiny damage in structures in the form of breathing crack. The simulation of the microcrack's effect on the response is essential for several damage identification targets. The conventional finite element method suffers from very small mesh size requirements to address the high-frequency problems, resulting in very large mass and stiffness matrices. In this study, the scaled boundary finite element method was applied to model different schemes of structural health monitoring of a structure with breathing cracks based on high-frequency vibration. The scaled boundary finite element method discretizes only the boundary of the model and thus substantially reduces the size of structural matrices. The node-to-node contact strategy was introduced to the scaled boundary finite element method to capture the contact problem that occurs during the vibration of the breathing crack. As breathing crack vibration results in some nonlinear effects, the simulation of three phenomena was of interest: higher harmonic generation, frequency shift, and vibro-acoustic modulation. A shooting method was used for efficient time integration and description of the frequency response function in the nonlinear regime. According to the results, the scaled boundary finite element method is of great power, efficiency, and accuracy to treat the contact problems, especially in high-frequency regimes. Moreover, the nonlinear methods provide certain advantages over the linear techniques in the early detection of incipient damage.

1. Introduction

Vibration response of structures that is typically used for their health monitoring has some superiority over methods based on frequency response. The damage effects better emerge in the frequency content of the dynamic response and open a category of monitoring methods called frequency methods (Giurgiutiu, 2007; Sepehry et al., 2014; Xu et al., 2019; Zhang et al., 2016). Increasing the excitation frequency decreases the wavelength to a comparable size with tiny damages and makes them detectable. Thus, high-frequency vibration-based health monitoring methods are of great importance for early detection of damage and more reliable estimation of the remaining useful life (Giurgiutiu, 2007; Sepehry et al., 2014).

The contact between breathing crack faces usually induces nonlinear effects in the vibration response of the host structure (He and Ng, 2017; Nandi and Neogy, 2002). This type of nonlinear behavior emerges in the frequency content of the system response in the form of subharmonic and higher harmonics (Trojniar et al., 2014), the linear or

[1]Faculty of Mechanical and Mechatronics Engineering, Shahrood University of Technology, Iran
[2]Dynamics Based Maintenance, Engineering Technology, University of Twente, Netherlands
[3]Amirkabir University of Technology, Iran
[4]Department of Mechanical Engineering, University of Maryland Baltimore County, USA

Corresponding author:
Firooz Bakhtiari-Nejad, Department of Mechanical Engineering, Amirkabir University of Technology, 427 Hafez Avenue, Tehran 19368-55858, Iran.
Email: fbnejad@umbc.edu

nonlinear shift of the peak frequencies (Jalali and Bonab, 2013; Matlack et al., 2015), and also modulation frequencies (Jhang, 2009). The last one (also called vibroacoustic modulation (VAM) in the literature) categorizes the breathing cracks as nonclassical nonlinearity sources. According to the previous studies, nonlinear symptoms of damage emerge much earlier than the linear ones. Hence, nonlinear metrics will assist in damage identification in the very early stages of progressive damage.

Generally, the types of nonlinear behavior of the structure are divided into two classical and nonclassical categories (Ostrovsky and Johnson, 2001). Classical nonlinearities, which include microstructural distortion, stress concentration, thermoelastic dependence, and large strains, emerge as the formation of higher harmonic generation (HHG) (Trojniar et al., 2014) or frequency shift (FS) (Jalali and Bonab, 2013; Matlack et al., 2015) in the frequency response function, whereas the nonclassical nonlinear behaviors mainly arise from the kissing contact (due to cracked edges or loose joints) (Guyer and Johnson, 1999) or the hysteresis damping factors in the structure (Guyer and Johnson, 2009). In the technical literature, various phenomena, such as contact acoustic nonlinearity (Solodov et al., 2002; Turnbull et al., 1995), the Luxemburg–Gorky effect (Zaitsev et al., 2002), the memory effect (Solodov and Korshak, 2001), and the VAM (Donskoy and Sutin, 1998; Motaharifar et al., 2019), are attributed to nonclassical nonlinear behavior of structures. The nonclassical nonlinearities in the frequency response spectrum of the structure are represented by the formation of higher and lower harmonics, frequency mixing, linear (first degree) resonant frequency transfer (Meo et al., 2008), and frequency modulation (Jhang, 2009).

The possibility to predict the dynamic response of the host structure to the high-frequency actuation would be of great importance in the damage identification procedure which is an inverse problem. The finite element method (FEM), as one of the most popular approaches in this regard, suffers from very fine mesh size (10–20 elements per wavelength) required for capturing the high-frequency response of the problem (Ha and Chang, 2009). It also leads to extremely large mass and stiffness matrices which make the solution very time-consuming. To address this drawback, spectral elements emerged that try to approximate the displacement field with more efficient shape functions (Ha and Chang, 2009; Sepehry et al., 2017a, 2017c). The time domain spectral FEM takes advantage of higher order polynomials for efficient approximation field and is of great interest in the steady state and transient wave field modeling. Although much more efficient than the FEM, they still need a lot of nodes on and within the intended domain for discretization which leads to large structural matrices. Frequency domain spectral methods, on the other hand, transform the governing equation to the frequency domain using the Fourier or wavelet transformation and solve it in

that domain with effective shape functions (Joglekar and Mitra, 2016). Although very efficient, they are limited to some very limited cases that an analytical solution could be found for the transformed spatial differential equation. Model order reduction has also been proposed by Sepehry et al. to reduce the size of the structural matrices even more (Sepehry et al., 2017c, 2018a). However, decreasing the computational costs in this field is still of great interest.

Nodes, used in the spectral FEM, are on the boundary and inside the element. This leads to huge structure matrices for a very large structure, whereas the scaled boundary finite element method (SBFEM) uses only the nodes on the boundary. Therefore, this method has very small matrices compared with the higher order FEM (Deeks and Wolf, 2002; Ooi et al., 2013; Song, 2009; Song and Wolf, 1997, 2000) and can be used for modeling high-frequency applications (Gravenkamp et al., 2012, 2015, 2017; Sepehry et al., 2018b). In the case of a simple structure, although the spectral method needs a lower number of degrees of freedom (DOFs) than the SBFEM (Gravenkamp et al., 2017), they proposed a model reduction method to decrease the DOFs used in the SBFEM in comparison with that used in the spectral method for high-frequency application (Gravenkamp et al., 2017). Also, they showed that the number of DOFs of the SBFEM was significantly lower than that of the spectral method for complex geometry (such as stress singularities and domains with different materials) which is common in structural health monitoring. Several works include static analysis of the crack (Song and Wolf, 1997, 2002), a contact model of the crack in the static analysis (Xing et al., 2018; Zhang et al., 2018), crack propagation (Ooi et al., 2012, 2013; Yang, 2006), piezoelectric material (Li et al., 2013a, 2013b; Man et al., 2014), and modeling of the crack in wave propagation (Gravenkamp et al., 2012, 2015) in the SBFEM.

Recently, many researchers have investigated the SBFEM (Chongshuai et al., 2018; Li et al., 2019; Song, 2004, 2009; Song et al., 2018; Zou et al., 2019; Wolf, 2002). The equation of singular stress at cracks by the SBFEM is derived by Song and Wolf, (2002). The dynamic stress intensity factors using the SBFEM were developed by Song (2004) and Yang et al. (2007).

The effect of opening–closing crack on the vibration of a structure was studied by Chatterjee (2010), Rezaee and Hassannejad (2011). Some works investigated a breathing crack using a fully open or fully closed crack (Chondros et al., 2001; Cheng et al., 1999; Lu et al., 2016; Nandi and Neogy, 2002; Rubio et al., 2017; Yang et al., 2010; Zhang and Li, 2014). Also, this type of crack was studied in the field of wave propagation using the FEM (Bouboulas and Anifantis, 2011; Friswell and Penny, 2002), the time domain spectral element method (He and Ng, 2017; Nandi and Neogy, 2002), and the wavelet spectral element method for the beam structure (Joglekar and Mitra, 2016). The nonlinear vibration of a dual-rotor system containing

a breathing transverse crack was investigated by Lu et al. (2016). Sepehry et al. (2017b) investigated the breathing crack modeling for the Euler–Bernoulli beam using the impedance method. Moreover, they showed that damping increased with the increase of frequency, and this leads to a decrease in the detection ability of damage in the frequency domain (Sepehry et al., 2017a).

In this study, a general formulation for the modeling of a tiny breathing crack in the SBFEM based on the node-to-node face contact strategy of a crack is developed. Because of the nonlinear nature of this phenomenon, the nonlinear frequency response of a 2D structure is calculated using the shooting method (Ibrahim et al., 2009; Nayfeh and Balachandran, 2008). In the following, three methods are used to detect an early crack in the vibration method including nonlinear frequency response of contact modeling of the crack using the shooting method, higher harmonics of one harmonic excitation, and VAM based on system excitation using two different frequencies. The results of the vibration of the breathing crack in the SBFEM are verified with the FEM. Moreover, the VAM is verified by the experimental result (Long et al., 2019). The obtained data using the three mentioned methods show that the linear methods, unlike nonlinear methods, cannot detect early damage.

2. Fundamentals of the SBFEM

A two-dimensional geometry of the domain is presented in Figure 1. The spectral element is used to discretize the boundaries of geometry. The radial coordinate (ξ) equals zero at the origin (scaling center) and one everywhere on the boundary. The coordinate η is the other local coordinate of the element. For the crack element, several works use the tip of crack as a scaling center (Ooi et al., 2012, 2013; Song and Wolf, 2002; Yang, 2006). In this study, a node-to-node strategy contact face is considered. The crack section of the structure is discretized as Figure 2. These nodes applied for the node-to-node contact strategy. The boundary discretization is interpolated by the set of shape functions $\mathbf{N}(\eta)$.

The Cartesian coordinates x_b and y_b are transformed to the scaled coordinates ξ and η as follows

$$x_b = \xi \mathbf{N}(\eta)x \tag{1}$$

$$y_b = \xi \mathbf{N}(\eta)y \tag{2}$$

where x and y represent the node coordinates. The displacement field is given as

$$\widehat{u}(\eta,\xi) = \mathbf{N}(\eta)u(\xi) \tag{3}$$

where $\widehat{u}(\eta,\xi)$ is the displacement field at a given location in the domain, and $u(\xi)$ is the displacement as a function of ξ corresponding to the nodes on the boundary.
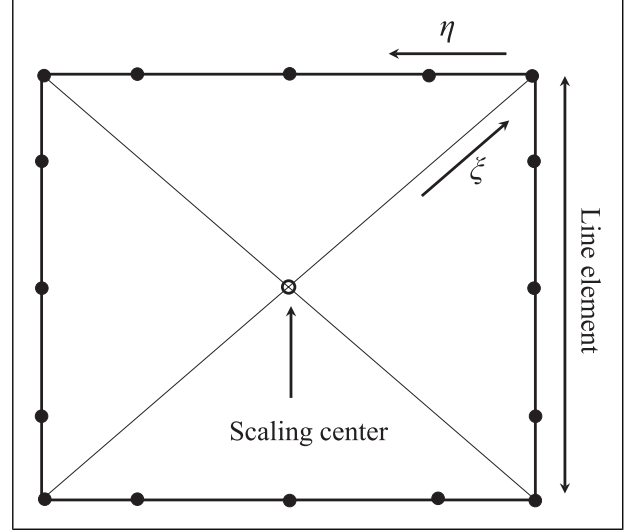

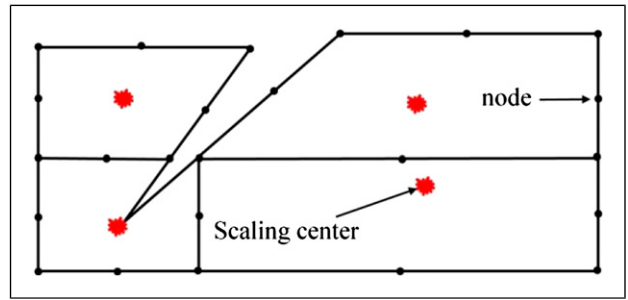**Figure 1.** Scaled boundary finite element method discretization of a simple subdomain.

Figure 2. Section of cracked structure with crack tip and crack faces with four subdomains.

After applying the virtual work principle (Deeks and Wolf, 2002) or weighted residual method (Song, 2009; Song and Wolf, 1997), the SBFEM is obtained as (Gravenkamp et al., 2017)

$$\mathbf{E}_0\xi^2 u_{,\xi\xi} + \left(\mathbf{E}_0 - \mathbf{E}_1 + \mathbf{E}_1^T\right)\xi u_{,\xi} - \mathbf{E}_2 u + \omega^2\xi^2\mathbf{M}_0 u = 0 \tag{4}$$

where $\mathbf{M}_0$ is the mass matrix of line element, ω is the frequency, and $\mathbf{E}_0, \mathbf{E}_1$, and $\mathbf{E}_2$ are defined as follows

$$\mathbf{E}_0 = \int_{-1}^{1} B_1^T \mathbf{D} B_1 |J| d\eta \tag{5}$$

$$\mathbf{E}_1 = \int_{-1}^{1} B_2^T \mathbf{D} B_1 |J| d\eta \tag{6}$$

$$\mathbf{E}_2 = \int_{-1}^{1} B_2^T \mathbf{D} B_2 |J| d\eta \tag{7}$$

$$\mathbf{M}_0 = \rho \int_{-1}^{1} \mathrm{N}^{\mathrm{T}} \mathbf{N} |J| d\eta \tag{8}$$

with the elasticity matrix $\mathbf{D}$ and ρ mass density. The Jacobian matrix is (Ooi et al., 2013)

$$|J| = (\mathbf{N}(\eta)\mathrm{x})\left(\mathbf{N}(\eta)_{,\eta}\mathrm{y}\right) - (\mathbf{N}(\eta)\mathrm{y})\left(\mathbf{N}(\eta)_{,\eta}\mathrm{x}\right) \tag{9}$$

And the matrices $\mathbf{B}_1$ and $\mathbf{B}_2$ are defined as (Gravenkamp et al., 2017)

$$\mathbf{B}_1 = \mathbf{b}_1 \mathbf{N}; \quad \mathbf{B}_2 = \mathbf{b}_2 \mathbf{N}_{,\eta} \tag{10}$$

where

$$\mathbf{b}_1 = \frac{1}{|J|} \begin{bmatrix} \mathrm{y}_{,\eta} & 0 \\ 0 & -\mathrm{x}_{,\eta} \\ -\mathrm{x}_{,\eta} & \mathrm{y}_{,\eta} \end{bmatrix}; \quad \mathbf{b}_2 = \frac{1}{|J|} \begin{bmatrix} -\mathrm{y} & 0 \\ 0 & \mathrm{x} \\ \mathrm{x} & -\mathrm{y} \end{bmatrix} \tag{11}$$

The dynamic stiffness matrix $\mathrm{S}(\omega)$ differential equation on the boundary can be derived (Gravenkamp et al., 2017; Song, 2009)

$$(\mathrm{S}(\omega) - \mathbf{E}_1)\mathbf{E}_0^{-1}\left(\mathrm{S}(\omega) - \mathbf{E}_1^{\mathrm{T}}\right) - \mathbf{E}_2 + \omega\mathrm{S}(\omega)_{,\omega} + \omega^2\mathbf{M}_0 = 0 \tag{12}$$

For high frequency, the dynamic stiffness matrix is obtained as (Song, 2009)

$$\mathrm{S}(\omega) = \mathbf{K} - \omega^2\mathbf{M} - \omega^4\left(\mathbf{S}_0^{(1)} - \omega^2\,\mathbf{S}_1^{(1)} - \omega^4\left(\mathbf{S}_0^{(2)} - \omega^2\,\mathbf{S}_1^{(2)} - \cdots - \omega^4\left(\mathbf{S}_0^{(M_{\mathrm{cf}})} - \omega^2\,\mathbf{S}_1^{(M_{\mathrm{cf}})} - \cdots - \right)^{-1}\right)^{-1}\right)^{-1} \tag{13}$$

where matrices K and M are derived for low frequency and by solving algebraic Riccati and Lyapunov equations (Gravenkamp et al., 2017; Li et al., 2013a; Song, 2009). The integer M_{cf} represents the order of the continued fraction expansion. The higher order terms $\mathrm{S}_0^{(i)}$ and $\mathrm{S}_1^{(i)}$ are defined in Song (2009). The matrices $\mathbf{X}^{(i)}$ are introduced for preconditioning (Chen et al., 2014); the dynamic stiffness is obtained as (Gravenkamp et al., 2014)

$$\mathrm{S}(\omega) = \mathbf{K} - \omega^2\mathbf{M} - \omega^4\mathbf{X}^{(1)}$$

$$\times \left(\mathbf{S}_0^{(1)} - \omega^2\,\mathbf{S}_1^{(1)} - \omega^4\mathbf{X}^{(2)}\left(\mathbf{S}_0^{(2)} - \omega^2\,\mathbf{S}_1^{(2)} - \cdots - \omega^4\mathbf{X}^{(M_{\mathrm{cf}})}\left(\mathbf{S}_0^{(M_{\mathrm{cf}})} - \omega^2\mathbf{S}_1^{(M_{\mathrm{cf}})}\right)^{-1}\left[\mathbf{X}^{(M_{\mathrm{cf}})}\right]^{\mathrm{T}}\right)^{-1}\left[\mathbf{X}^{(2)}\right]^{\mathrm{T}}\right)^{-1}\left[\mathbf{X}^{(1)}\right]^{\mathrm{T}} \tag{14}$$

Based on this expansion, an equation of motion in the frequency domain can be derived as (Gravenkamp et al., 2017)

$$\mathbf{K}_{\mathrm{h}}\mathbf{z}(\omega) - \omega^2\mathbf{M}_{\mathrm{h}}\mathbf{z}(\omega) = \mathbf{f}(\omega) \tag{15}$$

where

$$\mathbf{K}_{\mathrm{h}} = (\mathrm{diag})\left(\mathrm{K}, \mathrm{S}_0^{(1)}, \mathrm{S}_0^{(2)}, \ldots, \mathrm{S}_0^{(M_{\mathrm{cf}})}\right) \tag{16}$$

$$\mathbf{M}_{\mathrm{h}} = \begin{pmatrix} \mathrm{M} & -\mathrm{X}^{(1)} & 0 & \cdots & 0 \\ -\left[\mathrm{X}^{(1)}\right]^{\mathrm{T}} & \mathrm{S}_1^{(1)} & -\mathrm{X}^{(2)} & \cdots & 0 \\ 0 & -\left[\mathrm{X}^{(2)}\right]^{\mathrm{T}} & \mathrm{S}_1^{(2)} & \cdots & 0 \\ \vdots & \vdots & \vdots & \ddots & \vdots \\ 0 & 0 & 0 & \cdots & \mathrm{S}_1^{(M_{\mathrm{cf}})} \end{pmatrix} \tag{17}$$

$$\mathbf{z} = \begin{Bmatrix} \mathrm{u} \\ \mathrm{u}^{(1)} \\ \mathrm{u}^{(2)} \\ \vdots \\ \mathrm{u}^{(M_{\mathrm{cf}})} \end{Bmatrix} \tag{18}$$

$$\mathbf{f} = \begin{Bmatrix} \mathrm{R} \\ 0 \\ 0 \\ \vdots \\ 0 \end{Bmatrix} \tag{19}$$

The vector u is the nodal displacements on the boundary. The vectors $\mathrm{u}^{(1)}, \mathrm{u}^{(2)}, \ldots, \mathrm{u}^{(M_{\mathrm{cf}})}$ represent auxiliary variables associated with the higher order terms. After computing the dynamic stiffness and mass matrices for all subdomains, they can be assembled like conventional finite elements.

3. Modeling of contact dynamics

In this section, the SBFEM is used to model the constrained equation of motion with normal contact conditions. The solution of the contact problem involves the following steps: define proper contact conditions, find the constrained equation of motion, using a search algorithm to find points which are interacted with each other, and prevent the penetration (Zienkiewicz and Taylor, 2005). For

formulating the contact conditions and constrained equations of motion, many different methods can be used (Behzad et al., 2013). In this study, the Lagrange multiplier method is considered for the contact problem. For the implementation of the Lagrange multiplier method, the gap function is defined and then the variational procedure is used to enforce contact conditions to the equation of motion. Finally, implicit time integration is used as a numerical solution of nonlinear system equations.

3.1. Node-to-node contact method

According to Figure 2, the faces of the crack can be in contact with each other. On the other hand, the crack faces are discretized to obtain the numerical solution. The nodes on the one side of the crack are considered as slave nodes and those of the other side of the crack as master nodes. The distance between the crack faces does not penetrate by applying contact conditions. To determination of which "nodes" of one side of the crack penetrates the other side, the search algorithm is used. Because the one side of the crack may contact with several nodes of the other side, this approach is called "node-to-node."

3.2. Definition of the gap function

Points A and B in Figure 3 are the one node of the one side of the crack and one node of the other side of the crack. Let x_A and x_B be the current position vectors and u_A and u_B be the current displacement vectors of the points A and B, respectively. The normal gap function can be written as follows if A and B are considered the one nodal contact pair
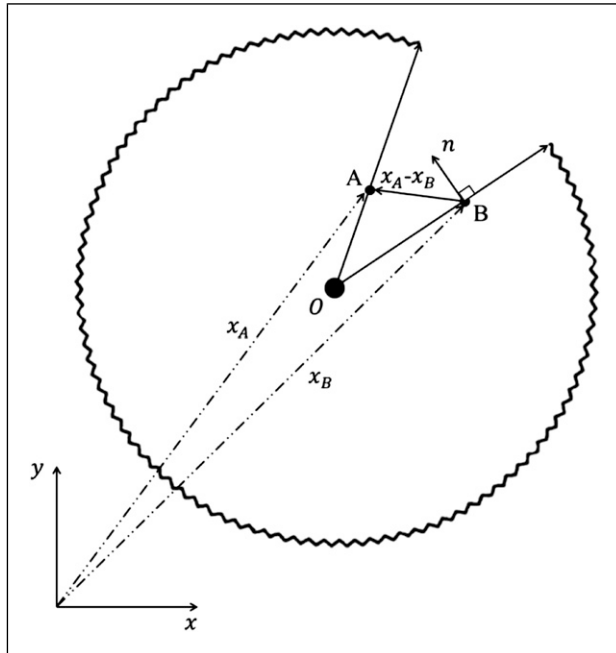

Figure 3. Gap function for the faces of the crack.

$$g_N = n^T(x_A - x_B) \qquad (20)$$

where n is the unit normal vector of the crack face of point B pointing to A and g_N is the normal gap function. The local contact matrix (G_L) could be written as

$$g_N = \begin{bmatrix} n_x & n_y & -n_x & -n_y \end{bmatrix} \begin{bmatrix} x_A \\ y_A \\ x_B \\ y_B \end{bmatrix} = [G_L] \begin{bmatrix} x_A \\ y_A \\ x_B \\ y_B \end{bmatrix} \qquad (21)$$

where x and y are the horizontal and vertical components of the position vector x, respectively. The global contact matrix (G_N) is obtained by assembling of the local contact matrix for all nodal contact pairs defined as (Behzad et al., 2013)

$$[G_N] = \left[\left[G_L^1 0 \right]^T \middle| \left[G_L^2 0 \right]^T \middle| \ldots \middle| \left[G_L^s 0 \right]^T \right]^T \qquad (22)$$

where s denotes the number of activated nodal contact pairs and G_L^i is the local contact matrix of ith nodal contact pair. So, the gap function can be defined as

$$g_N = G_N x = G_N(u + x_0) \qquad (23)$$

where u and x_0 are the initial displacement vectors and position of nodes, respectively.

3.3. Contact conditions

In this study, only the normal contact problem is studied. The contact conditions also famous as Hertz–Signorini–Moreau conditions (Wriggers and Zavarise, 2004) should make sure that: the penetration of the side faces of crack will not occur; if the normal gap is negative, then the gap will be zero else the gap is positive, and the normal contact force would be zero and described as

$$\begin{cases} g_N^i \geq 0 \\ p_N^i \leq 0 \\ p_N^i g_N^i = 0 \end{cases} \qquad \text{for} \quad i = 1, 2, \ldots, s \qquad (24)$$

where p_N^i for the ith nodal contact pair is the normal contact pressure.

3.4. Motion equation with constraints

The Lagrange multiplier method is used to add constraints to the equation. The variation of the energy related to the contact interface Γ_c without a slip condition is given by (Wriggers and Zavarise, 2004)

$$\delta\Pi_c = \int_{\Gamma_c} (p_N \delta g_N) dA + \int_{\Gamma_c} (g_N \delta p_N) dA \qquad (25)$$

where p_N is the pressure contact. By applying the node-to-node contact approach in the SBFEM discretization,

equation (28) for the s nodal contact pair is as follows (Wriggers and Zavarise, 2004)

$$\delta \Pi_c = \delta \mathbf{g}_N^T \lambda_N + \delta \lambda_N^T \mathbf{g}_N \qquad (26)$$

where $\lambda_N = \begin{bmatrix} \lambda_N^1 & \lambda_N^2 & \cdots & \lambda_N^s \end{bmatrix}^T$, $\mathbf{g}_N = \begin{bmatrix} g_N^1 & g_N^2 & \cdots & g_N^s \end{bmatrix}^T$, and λ_N^i for the ith nodal contact pair are the Lagrange multipliers. The potential energy of the contact inserts to the potential energy related to the elastic deformation; static deformation of the elastic bodies being in contact is as follows

$$\begin{cases} \mathbf{K}u + \mathbf{G}_N^T \lambda_N = f \\ \mathbf{g}_N \geq 0; \quad \lambda_N \leq 0; \quad \mathbf{g}_N \lambda_N^T = 0 \end{cases} \qquad (27)$$

where K is the stiffness matrix and f is the vector of body forces and surfacetractions. The dynamic deformation of the elastic bodies with contact is rewritten as follows

$$\begin{cases} \mathbf{M}\ddot{u} + \mathbf{C}\dot{u} + \mathbf{K}u + \mathbf{G}_N^T \lambda_N = f \\ \mathbf{G}_N(u + \mathbf{x}_0) \geq 0; \quad \lambda_N \leq 0; \quad \mathbf{g}_N \lambda_N^T = 0 \end{cases} \qquad (28)$$

where M and C are mass and stiffness matrices, respectively.

3.5. Time integration solution of motion equation in contact

The method of "forward increment Lagrange multiplier method" is used as a numerical solution (Carpenter et al., 1991). The equation of motion in time t^n is expressed by

$$\begin{cases} \mathbf{M}\ddot{u}^n + \mathbf{C}\dot{u}^n + \mathbf{K}u^n + \left(\mathbf{G}_N^{n+1}\right)^T \lambda_N^n = f^n \\ \mathbf{G}_N^{n+1}\left(u^{n+1} + \mathbf{x}_0\right) \geq 0 \end{cases} \qquad (29)$$

It is assumed that in the current time t^n, no contact is observed. So $\lambda_N^n = 0$ and the Newmark time integration is used to calculate the displacement (u_{exp}^{n+1}) at the next time (t^{n+1})

$$\mathbf{K}_{eff} u_{exp}^{n+1} = \mathbf{F}_{eff} \qquad (30)$$

where K_{eff} and F_{eff} are defined in Teixeira (2009). If in this step time gap function in equation (32) is positive, then $u^{n+1} = u_{exp}^{n+1}$. Otherwise, contact has occurred and λ_N^n should be calculated. So the displacement at time t^{n+1} is as follows

$$u^{n+1} = u_{exp}^{n+1} + u_{con} \qquad (31)$$

where u_{con} is a displacement corrected by the Lagrange multiplier vector. So according to equation (32), we have

$$\begin{cases} \mathbf{K}_{eff} u_{con} + \left(\mathbf{G}_N^{n+1}\right)^T \lambda_N^n = 0 \\ \mathbf{G}_N^{n+1}\left(u_{exp}^{n+1} + u_{con} + \mathbf{x}_0\right) = 0 \end{cases} \qquad (32)$$

By using equation (35), the Lagrange multiplier vector is calculated as

$$\lambda_N^n = -\mathbf{G}_N^{n+1}\mathbf{K}_{eff}^{-1}\left(\mathbf{G}_N^{n+1}\right)^T \left(\mathbf{G}_N^{n+1}\left(u_{exp}^{n+1} + \mathbf{x}_0\right)\right) \qquad (33)$$

Finally, u_{con} is calculated

$$u_{con} = -\mathbf{K}_{eff}^{-1}\left(\mathbf{G}_N^{n+1}\right)^T \lambda_N^n \qquad (34)$$

4. Shooting method

The nonlinear frequency response of the structure is calculated by the shooting method. For finding the periodic response of the nonlinear system equation, the shooting method is applied. For the system of second-order ordinary differential equations, this method is presented in Ibrahim et al. (2009); Ribeiro (2004). This method is also given here shortly. The shooting method aims to find the initial conditions which cause the periodic response. In this approach, the initial condition $\left(\begin{Bmatrix} u(0) \\ \dot{u}(0) \end{Bmatrix} = \mu\right)$ must be equal with the solution in $(t = T)$ as follows (Ibrahim et al., 2009)

$$\begin{Bmatrix} u(0) \\ \dot{u}(0) \end{Bmatrix} = \begin{Bmatrix} u(T, \mu; \omega_{ext}) \\ \dot{u}(T, \mu; \omega_{ext}) \end{Bmatrix} \qquad (35)$$

where $T = 2\pi/\omega_{ext}$ is the minimal period and ω_{ext} is the harmonic excitation of the system. For obtaining the nonlinear frequency response, period T is taken as an integer multiple of fundamental period. The initial condition μ is not known, so it must be corrected as

$$\begin{Bmatrix} u(T, \mu_0 + \Delta\mu; \omega_{ext}) \\ \dot{u}(T, \mu_0 + \Delta\mu; \omega_{ext}) \end{Bmatrix} - (\mu_0 + \Delta\mu) = 0 \qquad (36)$$

where μ_0 is the initial guess and $\Delta\mu$ is the correction. By using the Taylor series, equation (39) can be rewritten as

Table 1. Pseudocode for calculating of system equations.

| |
|---|
| 1. Guess initial condition μ_0 |
| 2. $t = 0$ |
| 3. Solve equation (30) |
| 4. Check equation (29), if contact occurred go to 6 else go to 5 |
| 5. Set $u^{n+1} = u_{exp}^{n+1}$ and go to 9 |
| 6. Calculate λ_n using equation (33) |
| 7. Calculate u_{con} using equation (34) |
| 8. Set $u^{n+1} = u_{exp}^{n+1} + u_{con}$ |
| 9. If $t^{n+1} = T$ go to 10 else go to 3 |
| 10. If $\begin{Bmatrix} u(0) \\ \dot{u}(0) \end{Bmatrix} = \begin{Bmatrix} u(T, \mu; \omega_{ext}) \\ \dot{u}(T, \mu; \omega_{ext}) \end{Bmatrix}$ go to 13 else go to 11 |
| 11. Calculate $\Delta\mu$ using equation (37) |
| 12. Update initial condition $(\mu_0 = \mu_0 + \Delta\mu)$ and go to 2 |
| 13. End |
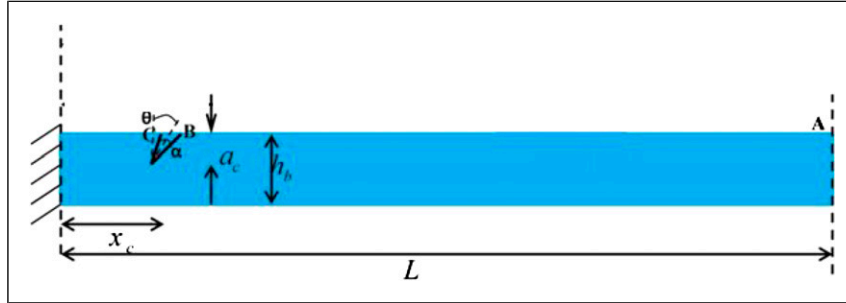
Figure 4. Schematic of the cantilever cracked 2D structure.

Table 2. Comparison of the displacement in the *y*-direction of the scaled boundary finite element method and the finite element method for force 1 N.

Point	p = 5, 2752 DOF	p = 7, 3884 DOF	p = 9, 5014 DOF	FEM, 58194 DOF	p_5 − FEM/FME × 100
A	-3.0231×10^{-7}	-3.0202×10^{-7}	-2.9791×10^{-7}	-2.9981×10^{-7}	0.83
B	-1.2947×10^{-7}	-1.2765×10^{-7}	-1.2527×10^{-7}	-1.2694×10^{-7}	2
C	-9.5942×10^{-8}	-9.5876×10^{-8}	-9.5777×10^{-7}	-9.5954×10^{-8}	−0.01

Note: FEM: finite element method; SBFEM: scaled boundary finite element method; DOF: degree of freedom.

Table 3. Comparison of the displacement in the *y*-direction of the scaled boundary finite element method and the finite element method for force 1 N.

Point	p = 5, 2752 DOF	p = 7, 3884 DOF	p = 9, 5014 DOF	FEM, 58194 DOF	p_5 − FEM/FME × 100
A	3.1602×10^{-5}	3.1511×10^{-5}	3.1224×10^{-5}	3.1401×10^{-5}	0.64
B	1.6365×10^{-6}	1.6345×10^{-6}	1.6321×10^{-6}	1.6364×10^{-6}	0.006
C	1.6364×10^{-6}	1.6344×10^{-6}	1.6320×10^{-6}	1.6362×10^{-6}	0.012

Note: FEM: finite element method; SBFEM: scaled boundary finite element method; DOF: degree of freedom.

Table 4. Comparison of the displacement in the *y*-direction of the scaled boundary finite element method and the finite element method for force 100 N.

Point	p = 5, 2752 DOF	p = 7, 3884 DOF	p = 9, 5014 DOF	FEM, 58194 DOF	p_5 − FEM/FME × 100
A	-2.8928×10^{-5}	-2.8905×10^{-5}	-2.8872×10^{-5}	-2.8933×10^{-5}	−0.017
B	-1.1619×10^{-5}	-1.1607×10^{-5}	-1.1592×10^{-5}	-1.1605×10^{-5}	0.12
C	-9.6191×10^{-6}	-9.6073×10^{-6}	-9.5923×10^{-6}	-9.6353×10^{-6}	−0.16

Note: FEM: finite element method; SBFEM: scaled boundary finite element method; DOF: degree of freedom.

Table 5. Comparison of the displacement in the *y*-direction of the scaled boundary finite element method and the finite element method for force 100 N.

Point	p = 5, 2752 DOF	p = 7, 3884 DOF	p = 9, 5014 DOF	FEM, 58194 DOF	p_5 − FEM/FME × 100
A	3.0532×10^{-3}	3.0503×10^{-3}	3.0465×10^{-3}	3.0535×10^{-3}	−0.01
B	1.6365×10^{-4}	1.6345×10^{-4}	1.6322×10^{-4}	1.6366×10^{-4}	−0.006
C	1.6364×10^{-4}	1.6344×10^{-4}	1.6321×10^{-4}	1.6365×10^{-4}	−0.006

Note: FEM: finite element method; SBFEM: scaled boundary finite element method; DOF: degree of freedom.

$$\left[\begin{array}{c} \dfrac{\partial \boldsymbol{u}}{\partial \boldsymbol{\mu}}(T, \boldsymbol{\mu}_0; \omega_{\text{ext}}) \\[2ex] \dfrac{\partial \dot{\boldsymbol{u}}}{\partial \boldsymbol{\mu}}(T, \boldsymbol{\mu}_0; \omega_{\text{ext}}) \end{array} - \mathbf{I} \right] \Delta \boldsymbol{\mu} = \boldsymbol{\mu}_0 - \left\{ \begin{array}{c} \boldsymbol{u}(T, \boldsymbol{\mu}_0; \omega_{\text{ext}}) \\[1ex] \dot{\boldsymbol{u}}(T, \boldsymbol{\mu}_0; \omega_{\text{ext}}) \end{array} \right\} \quad (37)$$

$$\left[\begin{array}{c} \dfrac{\partial \boldsymbol{u}}{\partial \boldsymbol{\mu}} \\[2ex] \dfrac{\partial \dot{\boldsymbol{u}}}{\partial \boldsymbol{\mu}} \end{array} \right]_{t=0} = \mathbf{I} \quad (38)$$

where I is the identity matrix. For the evaluation of $\partial \boldsymbol{u}/\partial \boldsymbol{\mu}$ and $\partial \dot{\boldsymbol{u}}/\partial \boldsymbol{\mu}$, it is not straightforward to differentiate equation (32); therefore, the finite difference method is used (Nayfeh and Balachandran, 2008) based on the following initial condition

The convergence of the shooting method is quadratic if the initial guess is close to the solution (Nayfeh and Balachandran, 2008).

The pseudocode for calculation of system equations based on the shooting method and time integration is presented in Table 1.
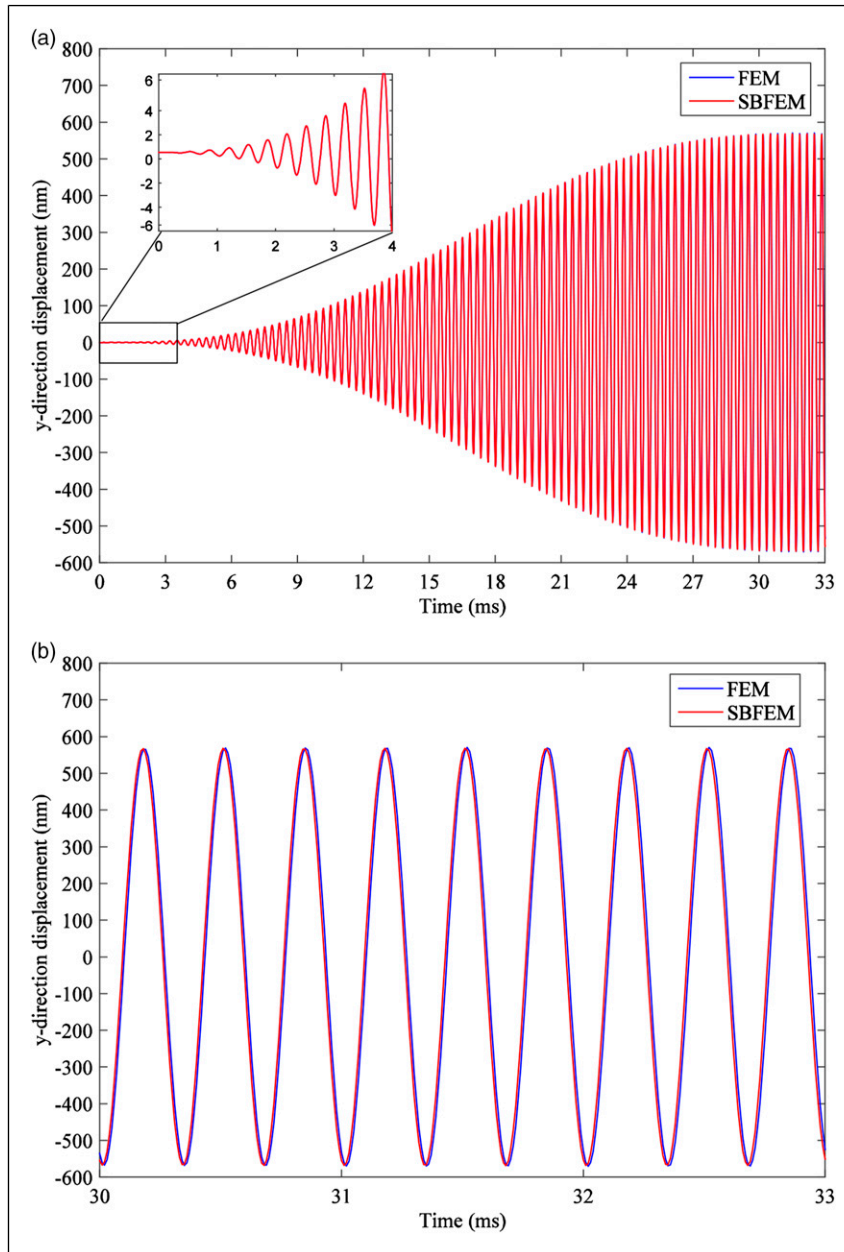

Figure 5. Comparison of the time history of cracked structure between the FEM and SBFEM for force 1 N. (a) 0–33 ms. (b) 30–33 ms. Note: FEM: finite element method; SBFEM: scaled boundary finite element method.

5. Results and discussion

5.1. Validation of the proposed method

The developed procedure to model the breathing crack using the SBFEM is validated for both static and dynamic solutions in this section. The response of a damaged structure to a static load at a certain point is studied in the static scheme to check the stiffness matrix extraction and assembly separately. For the dynamic solution, the eigenvalue analysis is performed to compute the eigenfrequencies and check them against a converged FE model

results. The time domain analysis is performed to validate the solution procedure presented in this section against the FEM results. Also, the proposed method result is confirmed using the experimental results of Long et al. (2019).

The configuration used to verify the applicability of the SBFEM for modeling crack is a 2D beam with a small V-shaped slit on it (Figure 4). The length and thickness of the beam are L = 400 mm and h = 5 mm. Isotropic material with the following properties is assumed as the constituent material: E = 70 GPa (Young's modulus), ρ = 2700 kg/m^3 (density), and ν = 0.3 (Poisson's ratio). The clamped
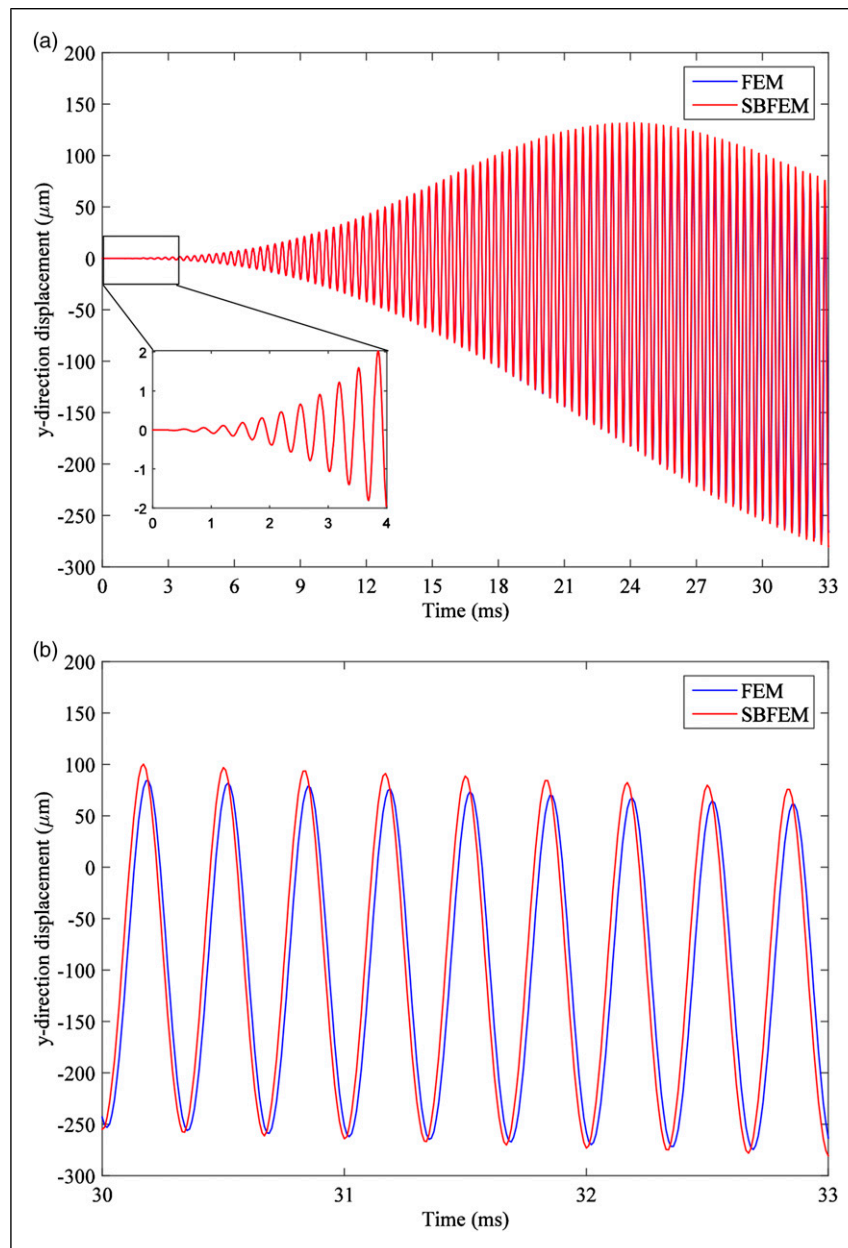

Figure 6. Comparison of the time history of cracked structure between the FEM and SBFEM for force 300 N. (a) 0–33 ms. (b) 30–33 ms.
Note: FEM: finite element method; SBFEM: scaled boundary finite element method.

boundary condition is applied at one end of the beam, and the other is free. The crack tip is located at 100 mm (x_c) from the fixed end, with the depth of 0.0025 mm from the top edge. The opening of the crack is specified using α = 0.06° and θ = 0°. In the static case, a force is applied at point A, and the results are gathered as the displacement of three points A, B, and C in Figure 4. Displacement results in the x- and y-direction are compared with the conventional FEM results in Tables 2–5 for 1 N (noncontact) and 100 N (contact) applied forces. The p-refinement (increasing the element order on the boundary nodes) is performed to investigate the convergence of the results through different polynomial degrees of the SBFEM and forces 1 N (noncontact) and 100 N (contact), respectively.

Finally, the displacement of point A is calculated for the dynamic force as follows

$$f = F \sin(2\pi f_c t)\left(1 - \cos\left(\frac{2\pi f_c}{n}\right)t\right) \quad (39)$$

where $f_c = 3000$ and n = 100. The results of two forces F = 1 N and 300 N applied in point A are compared with the commercial FEM and presented in Figures 5 and 6, respectively.

The some linear (noncontact) natural frequencies of the structure are presented in Table 6 for different polynomial degrees and with $M_{cf} = 1$.

For validation of the SBFEM with breathing crack, the result is compared with experimental results (Long et al., 2019). The dimension of the cantilever cracked beam is 406 mm × 12 mm, the crack depth is 3.8 mm, and the crack location is 176 mm. The Young modulus is 206 Gpa, density is 7850 kg/m³, and Poisson's ratio is ν = 0.3. For this model, a force is applied in point A, and the acceleration of point A in Figure 4 is calculated. The frequency of the applied force is $2f_1$, where $f_1 = 58.2$ is the fundamental natural frequency. The result is shown in Figure 7. According to this figure, a frequency modulation between fundamental frequency f_1 and exciting frequency $f_\omega = 2f_1$

Table 6. Comparison of the natural frequency (Hz) of the scaled boundary finite element method and the finite element method.

Mode	p = 5, 2752 DOF	p = 7, 3884 DOF	p = 9, 5014 DOF	FEM, 58194 DOF	$p_5 - FEM/FME \times 100$
1	24.643	24.628	24.800	24.6208	0.092
2	160.911	160.910	160.922	160.909	0.001
3	444.747	444.601	445.397	444.63	0.026
4	853.891	853.223	856.953	853.353	0.063
5	1417.326	1416.512	1421.080	1416.67	0.046
6	2150.495	2150.152	2151.949	2150.23	0.012
7	3006.460	3006.069	3007.685	3006.16	0.010
8	3099.337	3096.627	3111.312	3097.08	0.073
9	3930.735	3929.379	3936.716	3929.67	0.027
10	4963.642	4960.785	4976.877	4961.38	0.046
20	18338.579	18336.125	18324.659	18337.5	0.006
21	20137.118	20126.589	20169.344	20129.8	0.036
22	21894.697	21881.759	21939.504	21885.8	0.041
23	22458.509	22455.228	22461.429	22457.9	0.003
24	24711.481	24704.356	24713.056	24707.4	0.017
25	27345.556	27335.281	27305.233	27342.3	0.012
26	28155.690	28138.662	28205.056	28145.6	0.036
27	29919.705	29910.864	29863.303	29918	0.006
28	32034.836	32016.466	32066.360	32027.3	0.024
29	34038.594	34014.097	34074.495	34026.4	0.036
30	35081.695	35071.399	35061.556	35081.5	0.001
40	55363.949	55321.159	55073.518	55360	0.007
41	58304.745	58240.470	58281.628	58291.5	0.023
42	59228.239	59167.213	59250.206	59210.2	0.030
43	61352.939	61300.295	61074.920	61351.3	0.003
44	64029.528	63963.683	63473.836	64022	0.012
45	66156.888	66082.818	66058.672	66148.8	0.012
46	67906.430	67834.466	67196.383	67903.9	0.004

Note: FEM: finite element method; SBFEM: scaled boundary finite element method; DOF: degree of freedom.

was demonstrated as $f_1 + f_\omega$ in the SBFEM similar to experimental results.

5.2. Breathing crack detection for a rectangular 2D structure

5.2.1. Apply force and calculate the displacement of a 2D structure. In the first model, frequency response of point A vs. harmonics by applying a harmonic force for two forces 1 N and 300N in the cracked structure in point A is computed. Also, this result for force 1 N is calculated for the health structure. Figures 8 and 9 show these results for frequency excitations 3000 and 20140 Hz, respectively. Because of the dimension of the crack, this model could be used as a model of early crack detection.
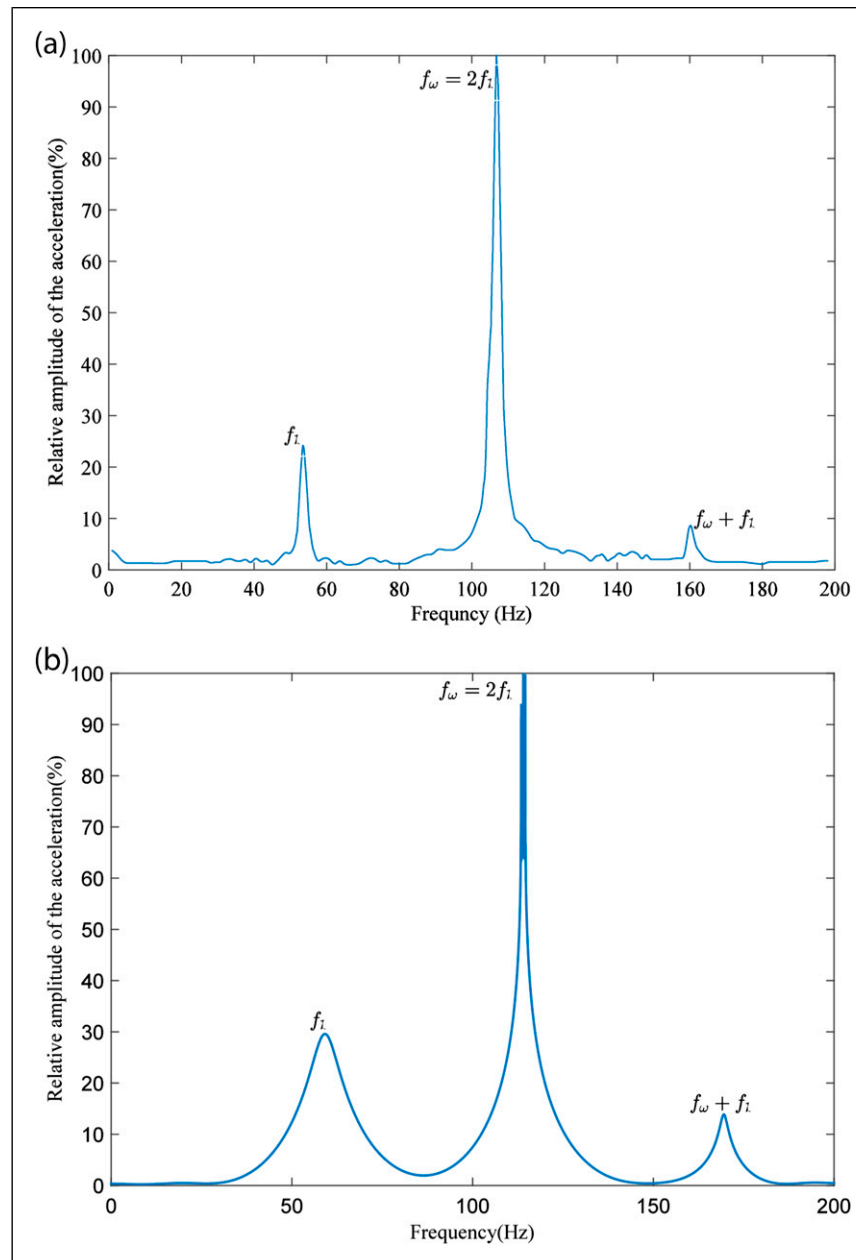

Figure 7. Comparison of the spectrum of cracked structure between (a) experimental results (Long et al., 2019) and (b) scaled boundary finite element method.
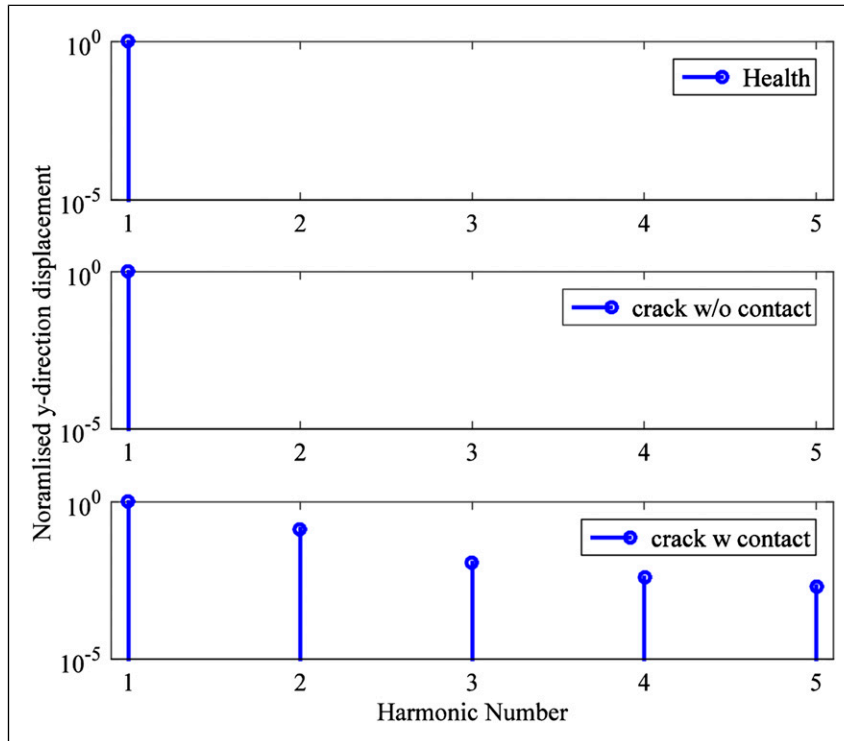
Figure 8. Displacement versus harmonic number for frequency 3000 Hz.
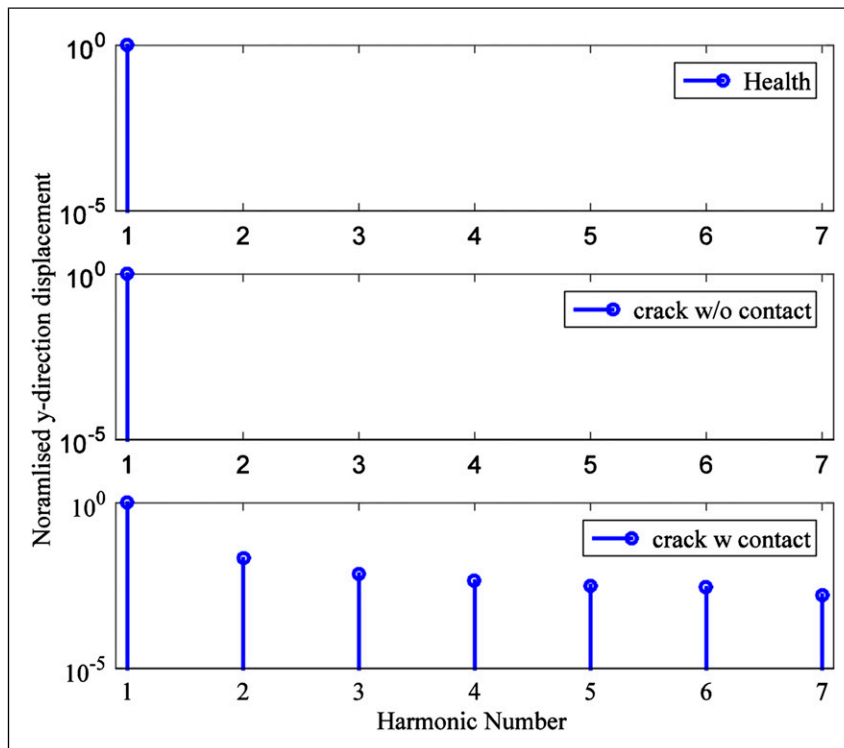

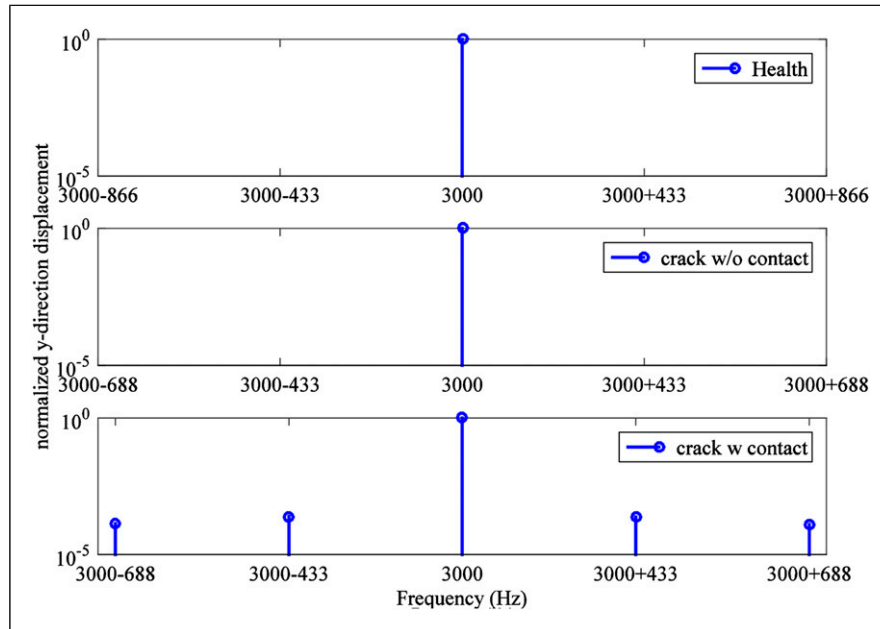**Figure 9.** Displacement versus harmonic number for frequency 20140 Hz.

Figure 10. Displacement versus harmonic number for the sum of two frequencies 433 Hz at 300 N and 3000 Hz at 1 N.

In these figures, the healthy and noncontact model only includes the first harmonic, but in contact model, higher harmonic also appeared. According to these figures, the early crack could be detected using a breathing model.

The sum of two forces with low and high frequencies is applied to point A. Figure 10 shows the results of the y-displacement of point A for the crack and health structure. The low frequency is 433 Hz with force 300N, and the high frequency is 3000 Hz with force 1 N. 433 Hz is selected because this frequency is near the natural frequency of the structure, and the less force is needed to the face of crack to be in contact.

The frequency response of the cracked structure is shown in Figure 11. This figure shows that in low force, the frequency response of the displacement is symmetric around the natural frequency of the structure. However, with increasing force, this symmetricity disappeared. This is because of the nonlinearity of contact phenomena. Therefore, this nonlinearity leads to unstable regions in frequency response. Also with increasing force, sub-harmonics appeared in the frequency response of the contact crack.

5.2.2. Breathing crack detection for a rectangular 2D structure with a hole.
In this section, the breathing crack of a rectangular 2D structure with the hole is studied. The model of the structure is presented in Figure 12.
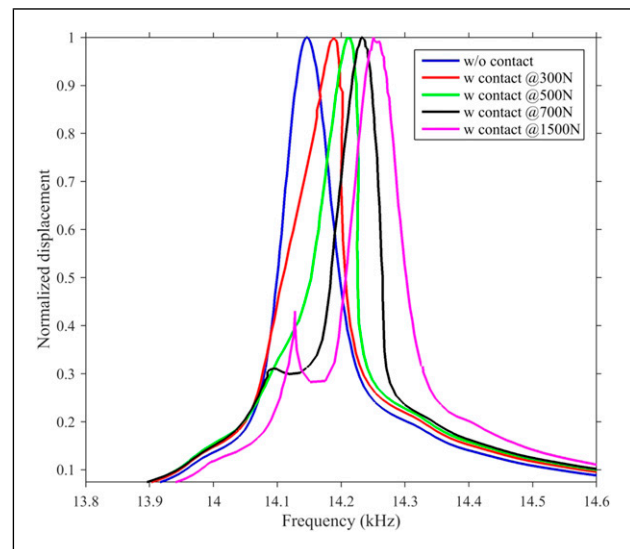

Figure 11. Frequency response for range 13.9–14.6 kHz for crack without contact and crack in contact with force 300 N, 500 N, 700 N, and 1500 N.

The dimension of the structure is 400 × 5 mm, and hole radius is 2.5 mm, and the hole location is $x_r = 65$ mm. The crack depth is 1.5 mm and $\alpha = 0.06°$. A force in point A in the y-direction is applied, and displacement of point A is calculated for the frequency 3000 Hz. The result of health and cracked structure 3000 Hz is presented in Figure 13.

Figure 12. Schematic of the cantilever cracked 2D structure with a hole.
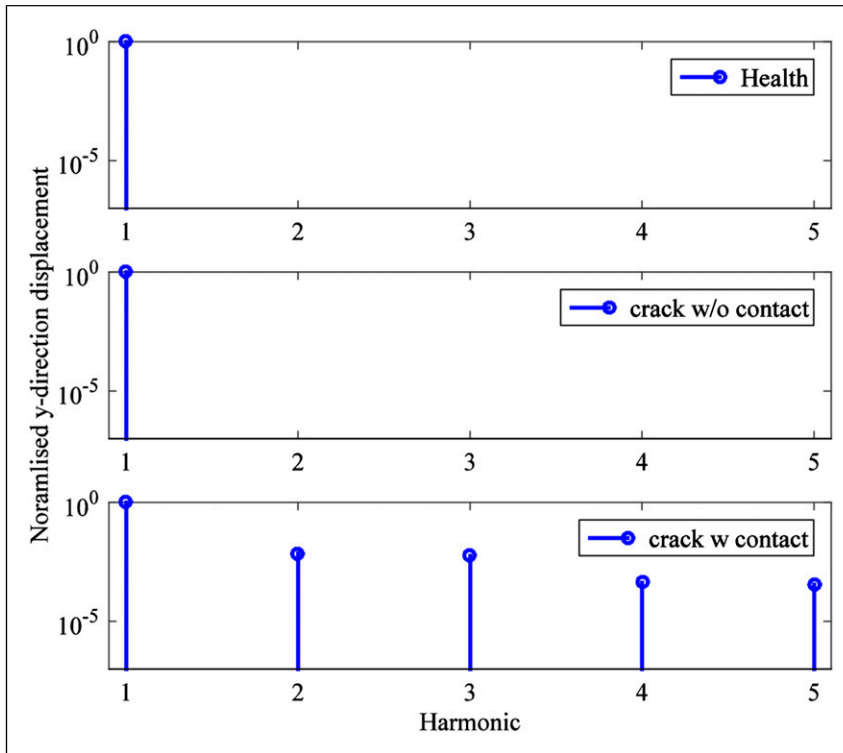

Figure 13. Displacement versus harmonic number for frequency 3000 Hz.

This figure also shows that nonlinear breathing crack is detected in the frequency response. However, nonbreathing is not distinct from the health structure.

6. Conclusion

The node-to-node contact strategy was introduced to the SBFEM for efficient modeling of the dynamic behavior of breathing cracks. The proposed method was implemented to simulate three common vibration-based health monitoring techniques: HHG, FS, and VAM. The shooting method was used to check the vibration regime effectively and to ensure that the steady-state regime has been achieved. The proposed method was verified against experimental and FEM results. The conformity of the SBFEM outcomes in all static, eigenfrequency, and time domain solutions with the FEM proved its ability to capture the contact problem with great accuracy. Comparing the number of DOFs in the SBFEM model with the FEM revealed the considerable efficiency of this method to reduce the computational time. It was also demonstrated that the SBFEM could effectively capture the HHG, FS, and VAM caused by nonlinear effects of the breathing crack. Therefore, the SBFEM is a promising approach that can facilitate and also improve the damage identification procedure.

Declaration of conflicting interests

ORCID iDs

Weidong Zhu ![ORCID] https://orcid.org/0000-0003-2707-2533
Firooz Bakhtiari-Nejad ![ORCID] https://orcid.org/0000-0002-7639-1242

References

Behzad M, Alvandi M, Mba D, et al. (2013) A finite element-based algorithm for rubbing induced vibration prediction in rotors. *Journal of Sound and Vibration* 332: 5523–5542.

Bouboulas A and Anifantis N (2011) Finite element modeling of a vibrating beam with a breathing crack: observations on crack detection. *Structural Health Monitoring: An International Journal* 10: 131–145.

Carpenter NJ, Taylor RL and Katona MG (1991) Lagrange constraints for transient finite element surface contact. *International Journal for Numerical Methods in Engineering* 32: 103–128.

Chatterjee A (2010) Structural damage assessment in a cantilever beam with a breathing crack using higher order frequency response functions. *Journal of Sound and Vibration* 329: 3325–3334.

Chen D, Birk C, Song C, et al. (2014) A high-order approach for modelling transient wave propagation problems using the scaled boundary finite element method. *International Journal for Numerical Methods in Engineering* 97: 937–959.

Cheng SM, Wu XJ, Wallace W (1999) Vibration response of a beam with a breathing crack. *Journal Sound and Vibration*. 225: 2018.

Chondros TG, Dimarogonas AD and Yao J (2001) Vibration of a beam with a breathing crack. *Journal of Sound and Vibration* 239: 57–67.

Chongshuai W, Yiqian H and Haitian Y (2018) Modelling the third kind boundary condition in scaled boundary finite element method based numerical analysis. *Engineering Analysis with Boundary Elements* 93: 53–62.

Deeks AJ and Wolf JP (2002) A virtual work derivation of the scaled boundary finite-element method for elastostatics. *Computational Mechanics* 28: 489–504.

Donskoy DM and Sutin AM (1998) Vibro-acoustic modulation nondestructive evaluation technique. *Journal of Intelligent Material Systems and Structures* 9: 765–771.

Friswell MI and Penny JET (2002) Crack modeling for structural health monitoring. *Structural Health Monitoring: An International Journal* 1: 139–148.

Giurgiutiu V (2007) *Structural Health Monitoring with Piezoelectric Wafer Active Sensors: with Piezoelectric Wafer Active Sensors*. Elsevier.

Gravenkamp H, Prager J, Saputra AA, et al. (2012) The simulation of lamb waves in a cracked plate using the scaled boundary finite element method. *The Journal of the Acoustical Society of America* 132: 1358–1367.

Gravenkamp H, Bause F and Song C (2014) On the computation of dispersion curves for axisymmetric elastic waveguides using the scaled boundary finite element method. *Computers & Structures* 131: 46–55.

Gravenkamp H, Birk C and Song C (2015) Simulation of elastic guided waves interacting with defects in arbitrarily long structures using the scaled boundary finite element method. *Journal of Computational Physics* 295: 438–455.

Gravenkamp H, Saputra AA, Song C, et al. (2017) Efficient wave propagation simulation on quadtree meshes using SBFEM with reduced modal basis. *International Journal for Numerical Methods in Engineering* 110: 1119–1141.

Guyer RA and Johnson PA (1999) Nonlinear mesoscopic elasticity: evidence for a new class of materials. *Physics Today* 52: 30–36.

Guyer RA and Johnson PA (2009) *Nonlinear Mesoscopic Elasticity: The Complex Behaviour of Rocks, Soil, Concrete*. John Wiley & Sons.

Ha S and Chang F-K (2009) Optimizing a spectral element for modeling PZT-induced Lamb wave propagation in thin plates. *Smart Materials and Structures* 19: 015015.

He S and Ng CT (2017) Modelling and analysis of nonlinear guided waves interaction at a breathing crack using time-domain spectral finite element method. *Smart Materials and Structures* 26: 085002.

Ibrahim SM, Patel BP and Nath Y (2009) Modified shooting approach to the non-linear periodic forced response of isotropic/composite curved beams. *International Journal of Non-Linear Mechanics* 44: 1073–1084.

Jalali H and Bonab BT (2013) Nonlinearity identification using sensitivity of frequency response functions. *Journal of Vibration and Control* 19: 787–800.

Jhang K-Y (2009) Nonlinear ultrasonic techniques for non-destructive assessment of micro damage in material: a review. *International Journal of Precision Engineering and Manufacturing* 10: 123–135.

Joglekar DM and Mitra M (2016) Analysis of flexural wave propagation through beams with a breathing crack using wavelet spectral finite element method. *Mechanical Systems and Signal Processing* 76–77: 576–591.

Li C, Man H, Song C, et al. (2013a) Analysis of cracks and notches in piezoelectric composites using scaled boundary finite element method. *Composite Structures* 101: 191–203.

Li C, Man H, Song C, et al. (2013b) Fracture analysis of piezoelectric materials using the scaled boundary finite element method. *Engineering Fracture Mechanics* 97: 52–71.

Li J, Shi Z and Liu L (2019) A scaled boundary finite element method for static and dynamic analyses of cylindrical shells. *Engineering Analysis with Boundary Elements* 98: 217–231.

Long H, Liu Y and Liu K (2019) Nonlinear vibration analysis of a beam with a breathing crack. *Applied Sciences* 9: 3874.

Lu Z, Hou L, Chen Y, et al. (2016) Nonlinear response analysis for a dual-rotor system with a breathing transverse crack in the hollow shaft. *Nonlinear Dynamics* 83: 169–185.

Man H, Song C, Gao W, et al. (2014) Semi-analytical analysis for piezoelectric plate using the scaled boundary finite-element method. *Computers & Structures* 137: 47–62.

Matlack K, Kim J-Y, Jacobs L, et al. (2015) Review of second harmonic generation measurement techniques for material state determination in metals. *Journal of Nondestructive Evaluation* 34: 273.

Meo M, Polimeno U and Zumpano G (2008) Detecting damage in composite material using nonlinear elastic wave spectroscopy methods. *Applied Composite Materials* 15: 115–126.

Motaharifar F, Ghassabi M and Talebitooti R (2019) Vibroacoustic behavior of a plate surrounded by a cavity containing an inclined part-through surface crack with arbitrary position. *Journal of Vibration and Control* 25: 2365–2379.

Nandi A and Neogy S (2002) Modelling of a beam with a breathing edge crack and some observations for crack detection. *Journal of Vibration and Control* 8: 673–693.

Nayfeh AH and Balachandran B (2008) *Applied Nonlinear Dynamics: Analytical, Computational, and Experimental Methods*. John Wiley & Sons.

Ooi ET, Song C, Tin-Loi F, et al. (2012) Polygon scaled boundary finite elements for crack propagation modelling. *International Journal for Numerical Methods in Engineering* 91: 319–342.

Ooi ET, Shi M, Song C, et al. (2013) Dynamic crack propagation simulation with scaled boundary polygon elements and automatic remeshing technique. *Engineering Fracture Mechanics* 106: 1–21.

Ostrovsky L and Johnson P (2001) Dynamic nonlinear elasticity in geo materials. *Rivista del Nuovo Cimento della Societa Italiana di Fisica* 24: 1–46.

Rezaee M and Hassannejad R (2011) A new approach to free vibration analysis of a beam with a breathing crack based on mechanical energy balance method. *Acta Mechanica Solida Sinica* 24: 185–194.

Ribeiro P (2004) Non-linear forced vibrations of thin/thick beams and plates by the finite element and shooting methods. *Computers & Structures* 82: 1413–1423.

Rubio P, Rubio L and Muñoz-Abella B (2017) Propagation of surface breathing cracks in shafts under quasi-static rotary bending. *Nonlinear Dynamics* 90: 1987–2000.

Sepehry N, Bakhtiari-Nejad F and Shamshirsaz M (2014) Thermo-electro-mechanical impedance based structural health monitoring of plates. *Composite Structures* 116: 147–164.

Sepehry N, Bakhtiari-Nejad F and Shamshirsaz M (2017a) Discrete singular convolution and spectral finite element method for predicting electromechanical impedance applied on rectangular plates. *Journal of Intelligent Material Systems and Structures* 28: 2473–2488.

Sepehry, N Bakhtiari-Nejad, F Shamshirsaz, M, et al. (2017b) Nonlinear modeling of cracked beams for impedance based structural health monitoring. In: ASME 2017 international mechanical engineering congress and exposition, Tampa, FL, 3–9 November 2017. USA: American Society of Mechanical Engineers (ASME).

Sepehry N, Shamshirsaz M and Bakhtiari Nejad F (2017c) Low-cost simulation using model order reduction in structural health monitoring: application of balanced proper orthogonal decomposition. *Structural Control and Health Monitoring* 24(11): e1994.

Sepehry N, Asadi S, Shamshirsaz M, et al. (2018a) A new model order reduction method based on global kernel k-means clustering: application in health monitoring of plate using lamb wave propagation and impedance method. *Structural Control and Health Monitoring* 25(9): e2211.

Sepehry N, Bakhtiari-Nejad F and Zhu W (2018b) Scaled boundary finite element method for modeling of impedance based structural health monitoring of 2D structure. In: ASME 2018 international design engineering technical conferences and computers and information in engineering, Quebec, Canada, 26–29 August 2018. Canada: American Society of Mechanical Engineers (ASME).

Solodov IY and Korshak BA (2001) Instability, chaos, and "memory" in acoustic-wave–crack interaction. *Physical Review Letters* 88: 014303.

Solodov IY, Krohn N and Busse G (2002) CAN: an example of nonclassical acoustic nonlinearity in solids. *Ultrasonics* 40: 621–625.

Song C (2004) A super-element for crack analysis in the time domain. *International Journal for Numerical Methods in Engineering* 61: 1332–1357.

Song C (2009) The scaled boundary finite element method in structural dynamics. *International Journal for Numerical Methods in Engineering* 77: 1139–1171.

Song C and Wolf JP (1997) The scaled boundary finite-element method-alias consistent infinitesimal finite-element cell method-for elastodynamics. *Computer Methods in Applied Mechanics and Engineering* 147: 329–355.

Song C and Wolf JP (2000) The scaled boundary finite-element method-a primer: solution procedures. *Computers & Structures* 78: 211–225.

Song C and Wolf JP (2002) Semi-analytical representation of stress singularities as occurring in cracks in anisotropic multi-materials with the scaled boundary finite-element method. *Computers & Structures* 80: 183–197.

Song C, Ooi ET, Pramod ALN, et al. (2018) A novel error indicator and an adaptive refinement technique using the scaled boundary finite element method. *Engineering Analysis with Boundary Elements* 94: 10–24.

Teixeira R (2009) *Computational Modelling of Structures using Discrete and Finite Elements*. PhD Thesis, Swansea University, United Kingdom.

Trojniar T, Klepka A, Pieczonka L, et al. (2014) Fatigue crack detection using nonlinear vibro–acoustic cross-modulations based on the Luxemburg–Gorky effect. In: Proceedings of SPIE health monitoring of structural and biological systems 2014, San Francisco, CA, 9 March 2014, pp. 90641F. USA: International Society for Optics and Photonics.

Turnbull PF, Perkins NC and Schultz WW (1995) Contact-induced nonlinearity in oscillating belts and webs. *Journal of Vibration and Control* 1: 459–479.

Wolf JP (2002) Response of unbounded soil in scaled boundary finite-element method. *Earthquake Engineering & Structural Dynamics* 31: 15–32.

Wriggers P and Zavarise G (2004) *Computational Contact Mechanics*. Encyclopedia of Computational Mechanics.

Xing W, Song C and Tin-Loi F (2018) A scaled boundary finite element based node-to-node scheme for 2D frictional contact problems. *Computer Methods in Applied Mechanics and Engineering* 333: 114–146.

Xu YF, Chen D-M and Zhu WD (2019) Operational modal analysis using lifted continuously scanning laser Doppler

vibrometer measurements and its application to baseline-free structural damage identification. *Journal of Vibration and Control* 25: 1341–1364.

Yang Z (2006) Fully automatic modelling of mixed-mode crack propagation using scaled boundary finite element method. *Engineering Fracture Mechanics* 73: 1711–1731.

Yang ZJ, Deeks AJ and Hao H (2007) Transient dynamic fracture analysis using scaled boundary finite element method: a frequency-domain approach. *Engineering Fracture Mechanics* 74: 669–687.

Yang Y, Ren X, Qin W, et al. (2010) Analysis on the nonlinear response of cracked rotor in hover flight. *Nonlinear Dynamics* 61: 183–192.

Zaitsev VY, Gusev V and Castagnède B (2002) Observation of the "Luxemburg–Gorky effect" for elastic waves. *Ultrasonics* 40: 627–631.

Zhang B and Li Y (2014) Six degrees of freedom coupled dynamic response of rotor with a transverse breathing crack. *Nonlinear Dynamics* 78: 1843–1861.

Zhang Z, Shankar K, Morozov EV, et al. (2016) Vibration-based delamination detection in composite beams through frequency changes. *Journal of Vibration and Control* 22: 496–512.

Zhang P, Du C, Tian X, et al. (2018) A scaled boundary finite element method for modelling crack face contact problems. *Computer Methods in Applied Mechanics and Engineering* 328: 431–451.

Tahtali OC and Taylor RL (2005) *The Finite Element Method for Solid and Structural Mechanics*. Elsevier.

Zou D, Teng X, Chen K, et al. (2019) A polyhedral scaled boundary finite element method for three-dimensional dynamic analysis of saturated porous media. *Engineering Analysis with Boundary Elements* 101: 343–359.